batteries

MDPI

Article

$NaBH_4$-Poly(Ethylene Oxide) Composite Electrolyte for All-Solid-State Na-Ion Batteries

Xiaoxuan Luo [1] and Kondo-Francois Aguey-Zinsou [2,*]

[1] MERLin, School of Chemical Engineering, The University of New South Wales, Sydney, NSW 2052, Australia; xiaoxuan.luo@unsw.edu.au
[2] MERLin, School of Chemistry, University of Sydney, Sydney, NSW 2006, Australia
* Correspondence: f.aguey@sydney.edu.au

Abstract: A disordered sodium borohydride ($NaBH_4$) environment to facilitate Na^+ mobility was achieved by partially hydrolyzing $NaBH_4$ and this significantly improved Na^+ ionic conductivity to 10^{-3} S cm^{-1} at 75 °C. The reaction rate of $NaBH_4$ self-hydrolysis, however, is determined by several parameters, including the reaction temperature, the molar ratio between $NaBH_4$ and H_2O, and the pH value; but these factors are hard to control. In this paper, poly(ethylene oxide) (PEO), capable of retaining H_2O through hydrogen bonding, was used in an attempt to better control the amount of H_2O available for $NaBH_4$ self-hydrolysis. This strategy led to the ionic conductivity of 1.6×10^{-3} S cm^{-1} at 45 °C with a Na^+ transference number of 0.54. The amorphous nature of the PEO matrix in hydrolyzed $NaBH_4$ is also believed to provide a conduction path for fast Na^+ conduction.

Keywords: composite electrolyte; complex borohydride; sodium borohydride; solid-state sodium electrolyte

check for updates

Citation: Luo, X.; Aguey-Zinsou, K.-F. $NaBH_4$-Poly(Ethylene Oxide) Composite Electrolyte for All-Solid-State Na-Ion Batteries. *Batteries* **2024**, *10*, 316. https://doi.org/10.3390/batteries10090316

Academic Editor: Yu Jiang

Received: 28 July 2024
Revised: 28 August 2024
Accepted: 3 September 2024
Published: 5 September 2024

1. Introduction

The feasibility of solid-state sodium (Na) ion batteries as the next generation of storage systems for large-scale renewable farms has attracted significant attention. Unlike lithium, sodium mineral deposits are more abundant, and easier to extract [1–3]. Ideally, new generations of Na-based batteries should not rely on organic electrolytes to remove any risk associated with their flammability [4,5]. A range of solid-state electrolytes has been investigated to address these safety issues [6,7].

Inorganic solid-state electrolytes, including NASICON ($Na_{1+x}Zr_2Si_xP_{3-x}O_{12}$) and sulfide ($Na_3PS_4$) electrolytes have acceptable ionic conductivities of 10^{-4}–10^{-3} S cm^{-1} at room temperature [8]. However, in NASICON electrolytes, the rigidity of the electrode/NASICON interface leads to high interface resistance, and as such a gradual degradation of the battery performance [9]. Sulfide-based electrolytes are also limited as they are sensitive to moisture, which leads to their decomposition and release of toxic H_2S gas [10].

Complex borohydrides are an emerging class of solid electrolytes for all-solid-state batteries as they have good electrochemical and thermal stability and ductility, which enables close contact between the electrode and electrolyte by simply cold pressing [11,12]. The advantages of sodium borohydride ($NaBH_4$) as a solid-state electrolyte include its high thermal stability (up to 500 °C) and good stability against metal anode [13–18]. However, the ionic conductivity of $NaBH_4$ is rather low (10^{-12} S cm^{-2} at 25 °C) [19].

To improve the ionic conductivity of $NaBH_4$, the pseudo-binary system consisting of the $NaBH_4$-NaI electrolyte was investigated. In this case, $Na(BH_4)_{1-x}I_x$ ($x = 5$) exhibited an ionic conductivity of 10^{-9} S cm^{-2} at 25 °C. Similarly, the formation of a solid solution between $Na(BH_4)$ and $Na(NH_2)$ led to an ionic conductivity of 2.0×10^{-6} S cm^{-1} at room temperature, and this improvement was attributed to the formation of the antiperovskite structure $Na(BH_4)_{0.5}(NH_2)_{0.5}$ with Na vacancies [13]. An alternative method to improve the ionic conductivity of $NaBH_4$ is through $NaBH_4$ surface oxidation [20]. Upon oxidation

of $NaBH_4$, Na vacancies can be created within the $NaBH_4$ crystalline structure, leading to an ionic conductivity of 2.5×10^{-3} S cm^{-1} at 35 °C. However, the level of $NaBH_4$ oxidation can be difficult to control [20].

PEO is often used to form composite electrolytes with sodium salts, such as $NaBF_4$ and $NaPF_6$ [21], and the ionic conductivity of the PEO-$NaPF_6$ electrolyte is 6.3×10^{-4} S cm^{-1} at 80 °C [22]. In PEO composite electrolytes, PEOs have the tendency to coordinate with Na salts because the polar ether group has a lone pair of electrons. This is believed to lead to Na^+ conduction paths whereby Na^+ successively coordinates and dissociates from the polar ether group, and as such, a high portion of the amorphous region in PEO composite electrolytes tends to deliver high ionic conductivity [23]. In the PEO-H_2O system, H_2O also forms, on average, 1.2 hydrogen bonds per repeating unit of PEO [24]. As such, by controlling the amount of PEO, the amount of H_2O hydrolyzing $NaBH_4$ can be better controlled. Herein, we report on a hydrolyzed PEO-$NaBH_4$-based composite electrolyte that achieved an ionic conductivity of 1.6×10^{-3} S cm^{-1} at 45 °C and demonstrated excellent electrochemical stability against Na metal anodes. This composite electrolyte also displayed a good Na^+ transference number (t_{Na+}) of 0.54 providing the possibility to build high-energy-density batteries [25].

2. Materials and Methods

All the operations were carried out under an inert atmosphere in an Argon-filled LC-Technology glove box (<1 ppm O_2 and H_2O). All chemicals were purchased from Sigma-Aldrich and stored in the glove box and this includes sodium borohydride ($NaBH_4$, 99%), PEO (Mv = 6×10^5), and diglyme (anhydrous, 99.5%). PEO was dried under a high vacuum for 24 h at 55 °C before use.

2.1. Synthesis of the Polymer Electrolyte

First, 5.3, 10.5, 21.0, and 31.5 mg of PEO were suspended in 5 mL diglyme in four separate bottles, respectively. Then 1.6, 3.5, 7.0, and 10.5 µL of Mili-Q H_2O was added dropwise to the PEO suspension containing 5.3, 10.5, 21.0, and 31.5 mg of PEO, respectively. The amount of H_2O added was calculated based on the amount of theoretical hydrogen bonds in PEO to precisely control the level of $NaBH_4$ hydrolysis. After stirring the mixtures overnight at 25 °C, 105 mg of $NaBH_4$ was added to each PEO suspension and further stirred for 6 h at 60 °C. After this, the suspensions were dried on a Schlenk line under a high vacuum at 10^{-3} mbar for 24 h at room temperature to lead to a dry white powder. The resulting materials were named according to the mass ratio between $NaBH_4$ and PEO, i.e., Hy-$NaBH_4$-5PEO refers to the mass of $NaBH_4$:PEO = 1:0.05. Other samples were named Hy-$NaBH_4$-10PEO, Hy-$NaBH_4$-20PEO, and Hy-$NaBH_4$-30PEO, accordingly.

2.2. Material Characterizations

The detailed measurement conditions for X-ray diffraction (XRD), X-ray photoelectron spectroscopy (XPS), Fourier transform infrared (FTIR) spectroscopy, thermogravimetric analysis (TGA), differential scanning calorimetry (DSC), and electrochemical impedance spectroscopy (EIS) were reported in Luo et al. [20,26].

2.3. Electrochemical Measurements

All electrochemical tests were performed in air-tight Swagelok cells on the SP-300 potentiostat at 45 °C. Linear sweep voltammetry (LSV) measurement was conducted with an asymmetric Na | Hy-$NaBH_4$-20PEO | SS cell at a scan rate of 0.1 mV s^{-1} from open circuit voltage (OCV) to 5 V. Na | Hy-$NaBH_4$-20PEO | Na cells were assembled and used for the galvanostatic and transference measurement. The symmetric cells were galvanostatically cycled at different C rates between −2 V and 2 V. The polarization voltage for Na^+ transference measurement was set at 10 mV with cell configuration of Na | Hy-$NaBH_4$-20PEO | Na.

3. Results

3.1. Characterization of Hy-$NaBH_4$-PEO Composite Electrolyte

The crystalline nature of Hy-$NaBH_4$-PEO was analyzed by XRD (Figure 1a). All the materials displayed diffraction peaks related to α-$NaBH_4$. The diffraction patterns of Hy-$NaBH_4$-5PEO, Hy-$NaBH_4$-10PEO, and Hy-$NaBH_4$-20PEO do not show any peaks related to crystalline PEO. However, at 30 wt% PEO, a peak at 2θ = 23° corresponding to crystalline PEO appeared. At higher PEO concentrations, additional peaks corresponding to crystalline $NaBO_2$ were also observed, including in Hy-$NaBH_4$-20PEO and Hy-$NaBH_4$-30PEO, and this confirmed that higher PEO amounts led to increased $NaBH_4$ hydrolysis. Higher amounts of PEO can bond more water molecules, which in turn facilitates the hydrolysis of $NaBH_4$ [26]. A broadening and shift of the $NaBH_4$ (200) peak to a lower 2θ value was also observed across all the materials (Figure 1b), and this may be due to the partial hydrolysis of $NaBH_4$ [27].

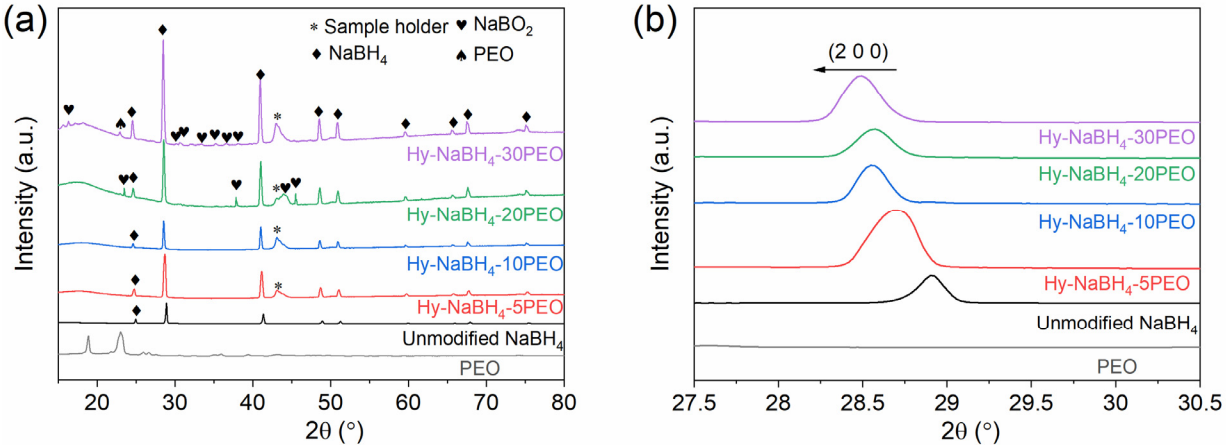

Figure 1. (**a**) X-ray diffraction XRD patterns of Hy-$NaBH_4$-5PEO, Hy-$NaBH_4$-10PEO, Hy-$NaBH_4$-20PEO, and Hy-$NaBH_4$-30PEO. Unmodified $NaBH_4$ and PEO are shown as references. (**b**) Enlarged view of the (200) peak for Hy-$NaBH_4$-5PEO, Hy-$NaBH_4$-10PEO, Hy-$NaBH_4$-20PEO, and Hy-$NaBH_4$-30PEO.

FTIR was used to identify the amorphous phases in Hy-$NaBH_4$-PEO as well as any chemical bonding between PEO and $NaBH_4$ (Figure 2). In Hy-$NaBH_4$-PEO, the typical B–H stretching modes shifted to higher wavenumbers, suggesting a strengthening of the BH bonds after PEO incorporation [28]. The absorption bands at 1602–1352 cm^{-1} were assigned to the asymmetric stretching modes of the BO_3 unit in $NaBO_2$ [29–31], confirming the partial oxidation of $NaBH_4$ in Hy-$NaBH_4$-PEO. A new vibration located at 937 cm^{-1} appeared in Hy-$NaBH_4$-PEO, and this was assigned to a lower symmetry of the tetrahedral BH_4^- anion as a result of the ion-pair interactions between PEO and the BH_4^- anion [32]. The stretching modes at 600–800 cm^{-1} appearing in Hy-$NaBH_4$-20PEO and Hy-$NaBH_4$-30PEO also suggested that higher amounts of $NaBO_2$ in the materials increased the level of hydrolysis [33,34].

The interaction of $NaBH_4$ with PEO was also evidenced by XPS analysis (Figure 3). B1s binding energy of 187.1 eV corresponding to $NaBH_4$ shifted to a lower value compared to unmodified $NaBH_4$ (187.7 eV). The same shift of $NaBH_4$ to lower binding energies was observed in the Na1s spectrum from 1072.1 to 1071.1 eV, and this was assigned to a weakening of the interaction between Na^+ and BH_4^- anions. This was interpreted as the result of the formation of the complex between $NaBH_4$ and PEO through the coordination of the ether oxygen in PEO with Na. Such an interaction may be the cause of the observed improvement in ionic conductivity observed in the composite PEO-$NaBH_4$ material.

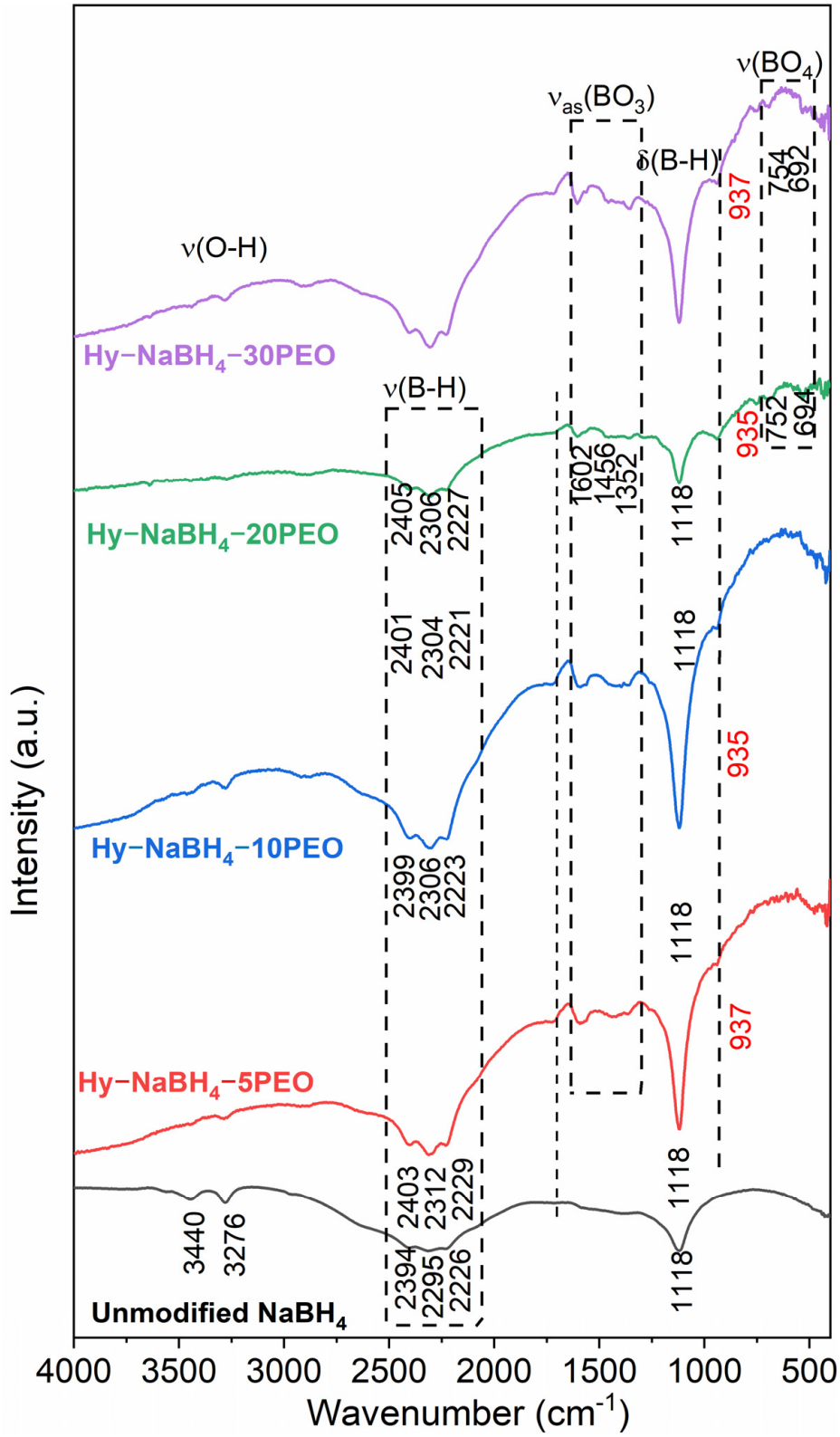

Figure 2. Fourier-transform infrared of Hy-$NaBH_4$-5PEO, Hy-$NaBH_4$-10PEO, Hy-$NaBH_4$-20PEO, and Hy-$NaBH_4$-30PEO. Unmodified $NaBH_4$ and PEO are shown as references.

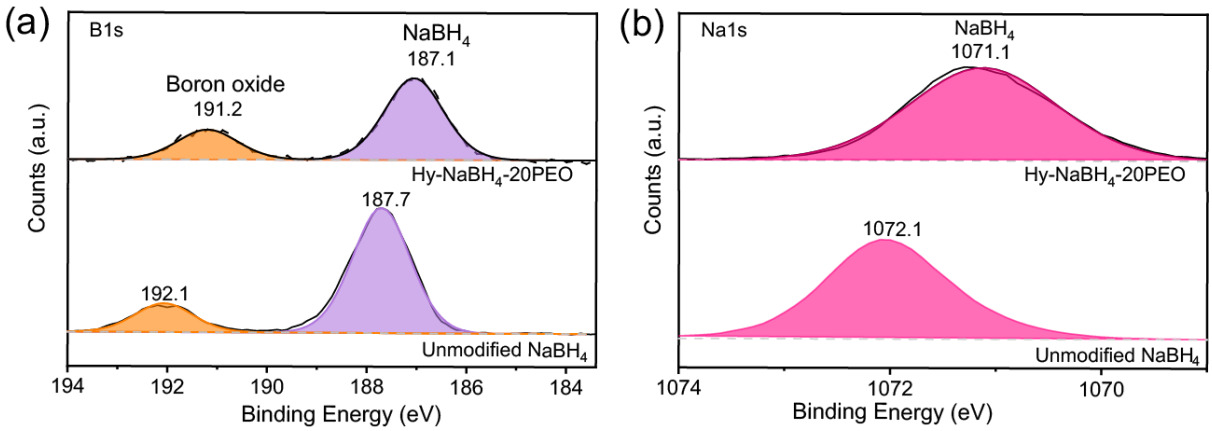

Figure 3. XPS of (**a**) B1s (**b**) Na1s of Hy-$NaBH_4$-20PEO and unmodified $NaBH_4$. The peak at 191.2 eV was assigned to the boron oxide phase [35,36].

3.2. Decrease in PEO Crystallinity in Hy-$NaBH_4$-PEO

In the composite electrolytes, ionic conductivity has been reported to mainly occur in the amorphous regions through local segmental motion [37]. The level of amorphous phase can be evidenced by DSC [38]. As such, the melting transition temperatures of PEO in the Hy-$NaBH_4$-PEO composites were thus analyzed by DSC (Figure 4). In PEO, the sharp endothermic peak located at 72.1 °C correlates with the melting of PEO [38,39]. For all Hy-$NaBH_4$-PEO materials, the melting point of PEO reduced from 72.1 °C to 42.1, 43.5, 44.4, and 45.3 °C with 5, 10, 20, and 30 wt% PEO, respectively, and this reflected an overall decrease in crystallinity of PEO [40,41]. The degree of crystallinity (χ_c) of the PEO in the composite electrolyte was calculated by using Equation (1) [42]:

$$\chi c = \frac{\Delta H_m}{\Delta H_{PEO}} \times 100\% \quad (1)$$

where ΔH_m is the melting enthalpy of Hy-$NaBH_4$-PEO and ΔH_{PEO} = 203 J g^{-1} [43] is the melting enthalpy of 100% crystalline PEO (Table A8.2). At the highest PEO loading (Hy-$NaBH_4$-30PEO), PEO crystallinity was the highest at 21.6%. However, in Hy-$NaBH_4$-5PEO, χ_c decreased to 10.7%, and this suggested a significant decrease in PEO crystallinity. The latter can be attributed to the steric interactions of Na^+ in $NaBH_4$ with the ether oxygen atoms in PEO, in agreement with previous observations in the $NaBF_4$-PEO complex [44–46].

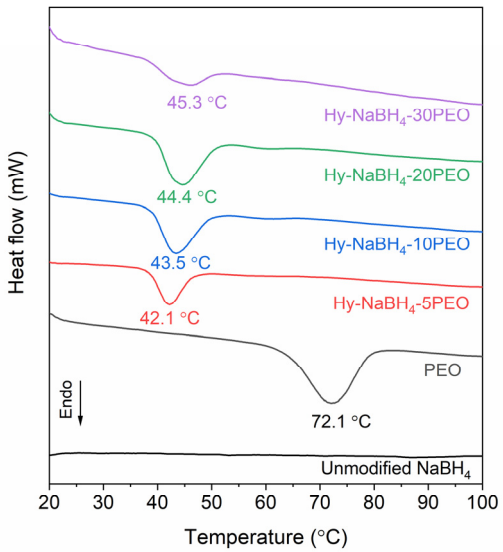

Figure 4. DSC of the Hy-$NaBH_4$-PEO composite electrolyte.

3.3. Electrochemical Properties of Hy-$NaBH_4$-PEO

The ionic conductivity of the Hy-$NaBH_4$-PEO composites was determined by EIS measurement and compared to the ionic conductivity of unmodified $NaBH_4$ (Figure 5a). All the materials show a significant increase in the ionic conductivity at room temperature compared to the ionic conductivity of unmodified $NaBH_4$ (1.4×10^{-10} S cm^{-1}). The Hy-$NaBH_4$-PEO materials also exhibited a jump in ionic conductivity at 45 °C, and this corresponds to the melting point of PEO as evidenced by DSC analysis (Figure 4). Hy-$NaBH_4$-20PEO exhibits the highest ionic conductivity of 4×10^{-6} S cm^{-1} at 25 °C, which is four times higher than unmodified $NaBH_4$. At 45 °C, the ionic conductivity in Hy-$NaBH_4$-20PEO increased to 1.6×10^{-3} S cm^{-1}. It should be noted that this value is comparable to the reported ionic conductivity of the widely investigated sulfide and NASICON electrolytes [2,47,48].

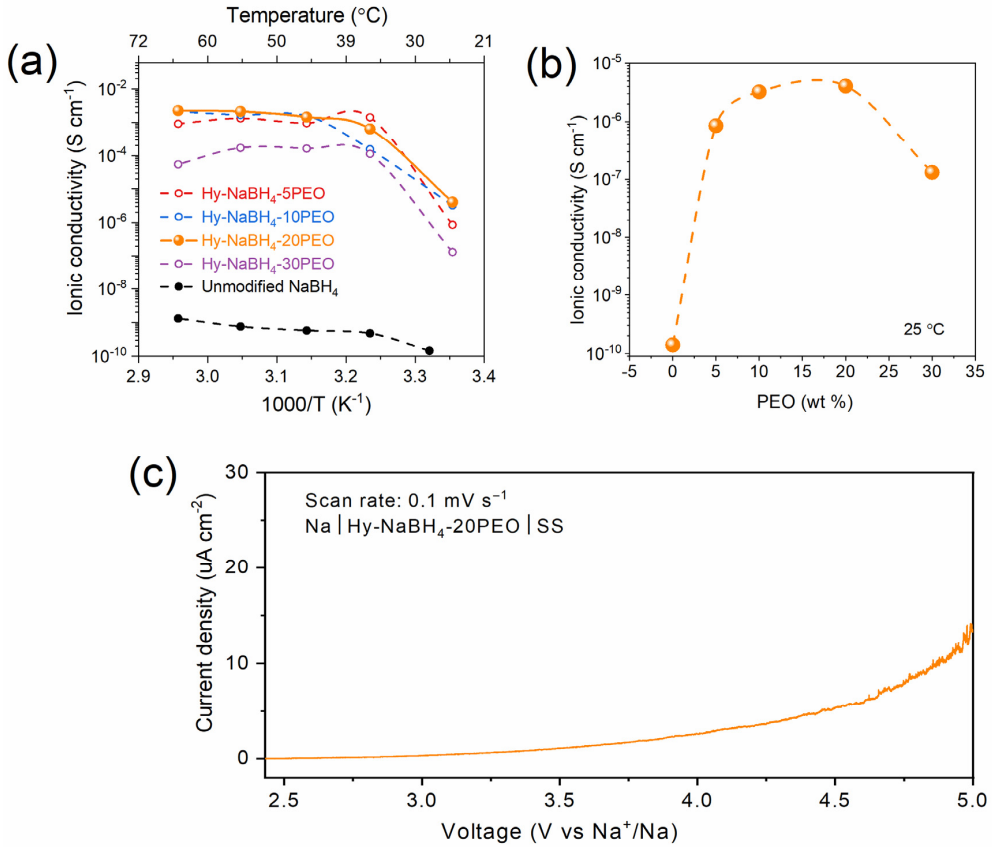

Figure 5. (**a**) Temperature dependence of the ionic conductivities of the Hy-$NaBH_4$-PEO materials and unmodified $NaBH_4$ shown as a reference; (**b**) correlation between the ionic conductivity of Hy-$NaBH_4$-PEO with respect to the PEO amount; (**c**) linear sweep voltammetry (LSV) curves from open circuit voltage to 5 V with a scan rate of 0.1 mV s^{-1} for Hy-$NaBH_4$-20PEO.

A correlation between the PEO amount and ionic conductivity of Hy-$NaBH_4$-PEO at 25 °C is shown in Figure 5b. The ionic conductivity of unmodified $NaBH_4$ is 10^{-10} S cm^{-1}, however, a significant increase in Na^+ conductivity to 8×10^{-7} S cm^{-1} is observed after the addition of 5% PEO. The conductivity increased by increasing the PEO amount and the maximum conductivity obtained was with 20 wt% PEO. However, by increasing the amount of PEO to 30 wt%, the ionic conductivity dropped to 1×10^{-7} S cm^{-1}. Based on the XRD and FTIR analysis, this decrease in ionic conductivity may be due to the presence of the crystalline $Na_2B_4O_7$ phase. In the case of Hy-$NaBH_4$-5PEO, the slightly lower ionic conductivity (Figure 5b) may be due to some trapping of the mobile cation due to the BH_4^- anion and PEO ion-pair interaction. Similar effects have been observed in PEO-$NaBH_4$/$NaBF_4$ electrolytes [49,50].

Owing to the high ionic conductivity of Hy-$NaBH_4$-20PEO at near room temperature, this material was further investigated. The transference number represents the effectiveness of Na^+ diffusion. A high transference number leads to a reduced concentration polarization at the electrolyte/electrode interface and thus higher power density [51–53]. The Na transference number (t_{Na+}) of Hy-$NaBH_4$-20PEO as a Na^+ electrolyte was measured using the DC polarization method. The current of the symmetrical cell under the polarization potential and the AC impedance spectra of the cell before/after polarization are shown in Figure S2. t_{Na+} calculated from the fitting results for Hy-PEO-20$NaBH_4$ was 0.54, which is higher than the commonly used PEO-NaTFSI solid-state electrolyte (0.2–0.4) [54]. This means that the use of Hy-PEO-20$NaBH_4$ as a solid-state electrolyte could potentially lead to a high-energy-density battery.

To demonstrate the feasibility of incorporating Hy-$NaBH_4$-20PEO into a Na-ion battery, the electrochemical stability window of Hy-$NaBH_4$-20PEO was measured by linear sweep voltammetry. An oxidative current corresponding to the electrolyte decomposition was observed around 3V (Figure 5c). This corresponds to an electrochemical stability window of 3 V, and, therefore, cathode materials such as $NaFePO_4$ could be used with Hy-$NaBH_4$-20PEO as the electrolyte [55].

To evaluate the long-term interface stability of Hy-$NaBH_4$-20PEO against Na metal. The symmetric cell was tested by galvanostatic cycling with the current density of 41 μA cm^{-2} at 45 °C. In the first cycle, the cell showed Na^+ plating/stripping with a voltage of 0.1 V/−0.1 V, and a gradual increase in overpotential is observed in the following Na plating/stripping. The cell shows a stable voltage (≈0.3 V) after the seventh plating. The gradual increase in overpotential during the initial cycling (Figure 6a) may be due to the partial decomposition of $BH4^-$ at the Na electrode interface, as reported in LiBH4 electrolytes [56,57]. Different current densities from 0.1 mA cm^{-2} to 0.2 mA cm^{-2} (20 min plating/20 min stripping) were applied to the galvanostatic cycling of the symmetric cell. The results (Figure 6b) show that the cell with the Hy-$NaBH_4$-20PEO electrolyte had reversible Na plating/stripping with a low overpotential (0.01 and 0.04 V, respectively), indicating that the electrolyte is compatible with Na metal anodes at a current density of 0.2 mA cm^{-2}.

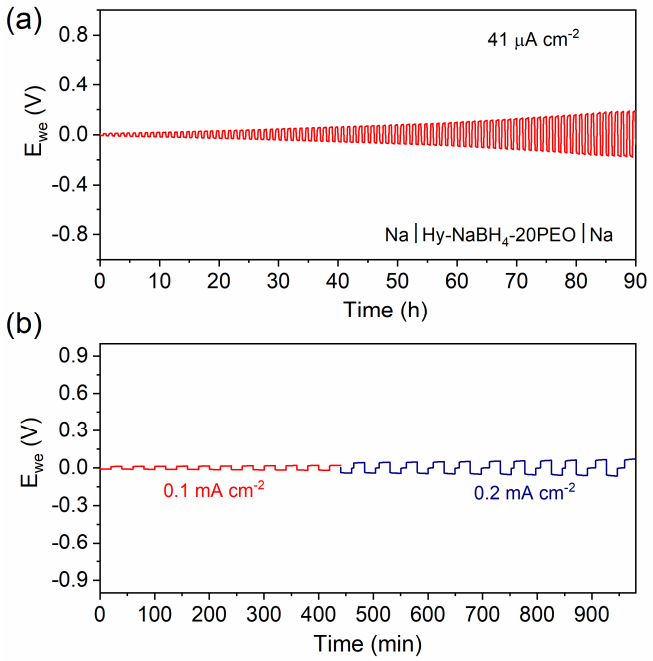

Figure 6. Voltage profiles during Na plating/stripping processes in (**a**) Na | Na symmetric cell with Hy-$NaBH_4$-20PEO as the electrolyte at a current density of 41 μA cm^{-2} at 45 °C, and (**b**) symmetric Na | Hy-$NaBH_4$-20PEO | Na cell cycled at various current densities of 0.1 and 0.2 mA cm^{-2} at 45 °C.

4. Conclusions

In this paper, we reported a Hy-$NaBH_4$-PEO composite electrolyte with an ionic conductivity of 1.6×10^{-3} S cm^{-2} at 45 °C, with a high transference number (0.54) and high electrochemical stability toward stable Na plating/stripping. By adding the PEO matrix, the level of $NaBH_4$ self-hydrolysis could be controlled by adjusting the PEO amount. Higher amounts of PEO increased the level of H_2O available to hydrolyze $NaBH_4$. In this Hy-$NaBH_4$-PEO composite electrolyte, the level of amorphous PEO is also believed to facilitate Na^+ mobility. Understanding the conduction mechanism of Hy-$NaBH_4$-PEO will help further increase the rate of Na^+ ionic conductivity at room temperature.

Supplementary Materials: The following supporting information can be downloaded at: https://www.mdpi.com/article/10.3390/batteries10090316/s1. References [58–63] are cited in the Supplementary Materials.

Author Contributions: X.L.: investigation, writing—original draft preparation, K.-F.A.-Z.: writing—review and editing, and supervision. All authors have read and agreed to the published version of the manuscript.

Funding: This research received no external funding.

Data Availability Statement: The data presented in this study are available on request from the corresponding author.

Conflicts of Interest: The authors declare no conflict of interest.

References

1. Yabuuchi, N.; Kubota, K.; Dahbi, M.; Komaba, S. Research Development on Sodium-Ion Batteries. *Chem. Rev.* **2014**, *114*, 11636–11682. [CrossRef] [PubMed]
2. Yang, C.; Xin, S.; Mai, L.; You, Y. Materials Design for High-Safety Sodium-Ion Battery. *Adv. Energy Mater.* **2021**, *11*, 2000974. [CrossRef]
3. Li, F.; Wei, Z.; Manthiram, A.; Feng, Y.; Ma, J.; Mai, L. Sodium-based batteries: From critical materials to battery systems. *J. Mater. Chem. A* **2019**, *7*, 9406–9431. [CrossRef]
4. Hwang, J.-Y.; Myung, S.-T.; Sun, Y.-K. Sodium-ion batteries: Present and future. *Chem. Soc. Rev.* **2017**, *46*, 3529–3614. [CrossRef] [PubMed]
5. Li, Y.; Sun, Z.; Jin, H.; Zhao, Y. Engineered Grain Boundary Enables the Room Temperature Solid-State Sodium Metal Batteries. *Batteries* **2023**, *9*, 252. [CrossRef]
6. Kim, J.-J.; Yoon, K.; Park, I.; Kang, K. Progress in the Development of Sodium-Ion Solid Electrolytes. *Small Methods* **2017**, *1*, 1700219. [CrossRef]
7. Li, Y.; Sun, C.; Sun, Z.; Li, M.; Jin, H.; Zhao, Y. Boosting Na-O Affinity in $Na_3Zr2Si_2PO_{12}$ Electrolyte Promises Highly Rechargeable Solid-State Sodium Batteries. *Adv. Funct. Mater.* **2024**, 2403937. [CrossRef]
8. Vasudevan, S.; Dwivedi, S.; Balaya, P. Overview and perspectives of solid electrolytes for sodium batteries. *Int. J. Appl. Ceram. Technol.* **2022**, *20*, 563–584. [CrossRef]
9. Li, Z.; Liu, P.; Zhu, K.; Zhang, Z.; Si, Y.; Wang, Y.; Jiao, L. Solid-State Electrolytes for Sodium Metal Batteries. *Energy Fuels* **2021**, *35*, 9063–9079. [CrossRef]
10. Zhang, L.; Yang, K.; Mi, J.; Lu, L.; Zhao, L.; Wang, L.; Li, Y.; Zeng, H. Na_3PSe_4: A Novel Chalcogenide Solid Electrolyte with High Ionic Conductivity. *Adv. Energy Mater.* **2015**, *5*, 1501294. [CrossRef]
11. Matsuo, M.; Orimo, S.-I. Lithium fast-ionic conduction in complex hydrides: Review and prospects. *Adv. Energy Mater.* **2011**, *1*, 161–172. [CrossRef]
12. Matsuo, M.; Remhof, A.; Martelli, P.; Caputo, R.; Ernst, M.; Miura, Y.; Sato, T.; Oguchi, H.; Maekawa, H.; Takamura, H.; et al. Complex Hydrides with $(BH_4)^-$ and $(NH_2)^-$ Anions as New Lithium Fast-Ion Conductors. *J. Am. Chem. Soc.* **2009**, *131*, 16389–16391. [CrossRef] [PubMed]
13. Matsuo, M.; Kuromoto, S.; Sato, T.; Oguchi, H.; Takamura, H.; Orimo, S.-I. Sodium ionic conduction in complex hydrides with $[BH_4]^-$ and $[NH_2]^-$ anions. *Appl. Phys. Lett.* **2012**, *100*, 203904. [CrossRef]
14. Unemoto, A.; Matsuo, M.; Orimo, S.I. Complex Hydrides for Electrochemical Energy Storage. *Adv. Funct. Mater.* **2014**, *24*, 2267–2279. [CrossRef]
15. Lu, Z.; Ciucci, F. Metal Borohydrides as Electrolytes for Solid-State Li, Na, Mg, and Ca Batteries: A First-Principles Study. *Chem. Mater.* **2017**, *29*, 9308–9319. [CrossRef]
16. de Kort, L.M.; Brandt Corstius, O.E.; Gulino, V.; Gurinov, A.; Baldus, M.; Ngene, P. Designing Highly Conductive Sodium-Based Metal Hydride Nanocomposites: Interplay between Hydride and Oxide Properties. *Adv. Funct. Mater.* **2023**, *33*, 2209122. [CrossRef]

17. Dou, Y.; Hansen, H.A.; Xu, S.-M.; Blanchard, D. Layered double hydroxides as advanced tracks to promote ionic conductivity in metal borohydride. *Mater. Chem. Front.* **2021**, *5*, 4989–4996. [CrossRef]
18. Duchêne, L.; Remhof, A.; Hagemann, H.; Battaglia, C. Status and prospects of hydroborate electrolytes for all-solid-state batteries. *Energy Storage Mater.* **2020**, *25*, 782–794. [CrossRef]
19. Luo, X.; Aguey-Zinsou, K.-F. Correlations between the ionic conductivity and cation size in complex borohydrides. *Ionics* **2020**, *26*, 5287–5291. [CrossRef]
20. Luo, X.; Rawal, A.; Cazorla, C.; Aguey-Zinsou, K.-F. Facile Self-Forming Superionic Conductors Based on Complex Borohydride Surface Oxidation. *Adv. Sustain. Syst.* **2020**, *4*, 1900113. [CrossRef]
21. Papke, B.L.; Ratner, M.A.; Shriver, D.F. Vibrational spectroscopy and structure of polymer electrolytes, poly(ethylene oxide) complexes of alkali metal salts. *J. Phys. Chem. Solids* **1981**, *42*, 493–500. [CrossRef]
22. Zhang, Q.; Lu, Y.; Yu, H.; Yang, G.; Liu, Q.; Wang, Z.; Chen, L.; Hu, Y.-S. PEO-$NaPF_6$ Blended Polymer Electrolyte for Solid State Sodium Battery. *J. Electrochem. Soc.* **2020**, *167*, 070523. [CrossRef]
23. Arya, A.; Sharma, A.L. Insights into the use of polyethylene oxide in energy storage/conversion devices: A critical review. *J. Phys. D Appl. Phys.* **2017**, *50*, 443002. [CrossRef]
24. Dahal, U.R.; Dormidontova, E.E. The dynamics of solvation dictates the conformation of polyethylene oxide in aqueous, isobutyric acid and binary solutions. *Phys. Chem. Chem. Phys.* **2017**, *19*, 9823–9832. [CrossRef]
25. Diederichsen, K.M.; McShane, E.J.; McCloskey, B.D. Promising Routes to a High Li^+ Transference Number Electrolyte for Lithium Ion Batteries. *ACS Energy Lett.* **2017**, *2*, 2563–2575. [CrossRef]
26. Dormidontova, E.E. Role of Competitive PEO-Water and Water-Water Hydrogen Bonding in Aqueous Solution PEO Behavior. *Macromolecules* **2002**, *35*, 987–1001. [CrossRef]
27. Luo, X.; Rawal, A.; Aguey-Zinsou, K.-F. Evidence of Superionic Na^+ Conductivity in Partially Hydrolyzed $NaBH_4$. *J. Phys. Chem. C* **2024**. [CrossRef]
28. Ahiavi, E.; Dawson, J.A.; Kudu, U.; Courty, M.; Islam, M.S.; Clemens, O.; Masquelier, C.; Famprikis, T. Mechanochemical synthesis and ion transport properties of Na3OX (X = Cl, Br, I and BH4) antiperovskite solid electrolytes. *J. Power Sources* **2020**, *471*, 228489. [CrossRef]
29. Zhu, Y.; Ouyang, L.; Zhong, H.; Liu, J.; Wang, H.; Shao, H.; Huang, Z.; Zhu, M. Closing the Loop for Hydrogen Storage: Facile Regeneration of $NaBH_4$ from its Hydrolytic Product. *Angew. Chem. Int. Ed.* **2020**, *59*, 8623–8629. [CrossRef]
30. Le, T.T.; Pistidda, C.; Puszkiel, J.; Milanese, C.; Garroni, S.; Emmler, T.; Capurso, G.; Gizer, G.; Klassen, T.; Dornheim, M. Efficient Synthesis of Alkali Borohydrides from Mechanochemical Reduction of Borates Using Magnesium-Aluminum-Based Waste. *Metals* **2019**, *9*, 1061. [CrossRef]
31. Saddeek, Y.B.; Aly, K.A.; Shaaban, K.S.; Ali, A.M.; Sayed, M.A. Elastic, optical and structural features of wide range of CdO-$Na_2B_4O_7$ glasses. *Mater. Res. Express* **2018**, *5*, 065204. [CrossRef]
32. Dupon, R.; Papke, B.L.; Ratner, M.A.; Whitmore, D.H.; Shriver, D.F. Influence of ion pairing on cation transport in the polymer electrolytes formed by poly(ethylene oxide) with sodium tetrafluoroborate and sodium tetrahydroborate. *J. Am. Chem. Soc.* **1982**, *104*, 6247–6251. [CrossRef]
33. Anghel, E.M.; Zaharescu, M.; Zuca, S.; Pavlatou, E. Structure and phase diagram of the $Na_2B_4O_7$-Na_3AlF_6 system. *J. Mater. Sci.* **1999**, *34*, 3923–3929. [CrossRef]
34. Dwivedi, B.P.; Khanna, B.N. Cation dependence of raman scattering in alkali borate glasses. *J. Phys. Chem. Solids* **1995**, *56*, 39–49. [CrossRef]
35. Luo, X.; Rawal, A.; Salman, M.S.; Aguey-Zinsou, K.-F. Core-Shell $NaBH_4$@$Na_2B_{12}H_{12}$ Nanoparticles as Fast Ionic Conductors for Sodium-Ion Batteries. *ACS Appl. Nano Mater.* **2022**, *5*, 373–379. [CrossRef]
36. Xie, W.; Zou, C.; Tang, Z.; Fu, H.; Zhu, X.; Kuang, J.; Deng, Y. Well-crystallized borax prepared from boron-bearing tailings by sodium roasting and pressure leaching. *RSC Adv.* **2017**, *7*, 31042–31048. [CrossRef]
37. Li, Z.; Fu, J.; Zhou, X.; Gui, S.; Wei, L.; Yang, H.; Li, H.; Guo, X. Ionic Conduction in Polymer-Based Solid Electrolytes. *Adv. Sci.* **2023**, *10*, 2201718. [CrossRef]
38. Kumar, B.; Rodrigues, S.J.; Koka, S. The crystalline to amorphous transition in PEO-based composite electrolytes: Role of lithium salts. *Electrochim. Acta* **2002**, *47*, 4125–4131. [CrossRef]
39. Liu, K.; Zhang, R.; Sun, J.; Wu, M.; Zhao, T. Polyoxyethylene (PEO) | PEO–Perovskite | PEO Composite Electrolyte for All-Solid-State Lithium Metal Batteries. *ACS Appl. Mater. Interfaces* **2019**, *11*, 46930–46937. [CrossRef]
40. Hou, H.; Xu, Q.; Pang, Y.; Li, L.; Wang, J.; Zhang, C.; Sun, C. Efficient Storing Energy Harvested by Triboelectric Nanogenerators Using a Safe and Durable All-Solid-State Sodium-Ion Battery. *Adv. Sci.* **2017**, *4*, 1700072. [CrossRef]
41. Hayashi, A.; Noi, K.; Sakuda, A.; Tatsumisago, M. Superionic glass-ceramic electrolytes for room-temperature rechargeable sodium batteries. *Nat. Commun.* **2012**, *3*, 856. [CrossRef] [PubMed]
42. Kuo, M.C.; Huang, J.C.; Chen, M. Non-isothermal crystallization kinetic behavior of alumina nanoparticle filled poly(ether ether ketone). *Mater. Chem. Phys.* **2006**, *99*, 258–268. [CrossRef]
43. Devi, C.; Gellanki, J.; Pettersson, H.; Kumar, S. High sodium ionic conductivity in PEO/PVP solid polymer electrolytes with InAs nanowire fillers. *Sci. Rep.* **2021**, *11*, 20180. [CrossRef]
44. Wang, C.; Wang, T.; Wang, L.; Hu, Z.; Cui, Z.; Li, J.; Dong, S.; Zhou, X.; Cui, G. Differentiated Lithium Salt Design for Multilayered PEO Electrolyte Enables a High-Voltage Solid-State Lithium Metal Battery. *Adv. Sci.* **2019**, *6*, 1901036. [CrossRef] [PubMed]

45. Wang, C.; Yang, T.; Zhang, W.; Huang, H.; Gan, Y.; Xia, Y.; He, X.; Zhang, J. Hydrogen bonding enhanced SiO_2/PEO composite electrolytes for solid-state lithium batteries. *J. Mater. Chem. A* **2022**, *10*, 3400–3408. [CrossRef]
46. Roy, A.; Dutta, B.; Bhattacharya, S. Ion dynamics in $NaBF_4$ salt-complexed PVC–PEO blend polymer electrolytes: Correlation between average ion hopping length and network structure. *Ionics* **2017**, *23*, 3389–3399. [CrossRef]
47. Wu, F.; Fitzhugh, W.; Ye, L.; Ning, J.; Li, X. Advanced sulfide solid electrolyte by core-shell structural design. *Nat. Commun.* **2018**, *9*, 4037. [CrossRef]
48. Lu, X.; Xia, G.; Lemmon, J.P.; Yang, Z. Advanced materials for sodium-beta alumina batteries: Status, challenges and perspectives. *J. Power Sources* **2010**, *195*, 2431–2442. [CrossRef]
49. Jaipal Reddy, M.; Chu, P.P. Ion pair formation and its effect in PEO:Mg solid polymer electrolyte system. *J. Power Sources* **2002**, *109*, 340–346. [CrossRef]
50. Papke, B.L.; Dupon, R.; Ratner, M.A.; Shriver, D.F. Ion-pairing in polyether solid electrolytes and its influence on ion transport. *Solid State Ion.* **1981**, *5*, 685–688. [CrossRef]
51. Lu, Y.; Li, L.; Zhang, Q.; Niu, Z.; Chen, J. Electrolyte and Interface Engineering for Solid-State Sodium Batteries. *Joule* **2018**, *2*, 1747–1770. [CrossRef]
52. Lu, Y.; Li, L.; Zhang, Q.; Cai, Y.; Ni, Y.; Chen, J. High-performance all-solid-state electrolyte for sodium batteries enabled by the interaction between the anion in salt and Na_3SbS_4. *Chem. Sci.* **2022**, *13*, 3416–3423. [CrossRef] [PubMed]
53. Thomas, K.E.; Sloop, S.E.; Kerr, J.B.; Newman, J. Comparison of lithium-polymer cell performance with unity and nonunity transference numbers. *J. Power Sources* **2000**, *89*, 132–138. [CrossRef]
54. Serra Moreno, J.; Armand, M.; Berman, M.B.; Greenbaum, S.G.; Scrosati, B.; Panero, S. Composite PEOn:NaTFSI polymer electrolyte: Preparation, thermal and electrochemical characterization. *J. Power Sources* **2014**, *248*, 695–702. [CrossRef]
55. Liao, H.; Zhang, Z.; Zheng, Y.; Gao, Y. $NaFePO_4$ for sodium-ion batteries: Mechanism, synthesis and optimization strategies toward commercialization. *Energy Storage Mater.* **2024**, *65*, 103157. [CrossRef]
56. Asakura, R.; Remhof, A.; Battaglia, C. Hydroborate-Based Solid Electrolytes for All-Solid-State Batteries. In *Solid State Batteries Volume 1: Emerging Materials and Applications*; American Chemical Society: Washington, DC, USA, 2022; Volume 1413, pp. 353–393.
57. Unemoto, A.; Ikeshoji, T.; Yasaku, S.; Matsuo, M.; Stavila, V.; Udovic, T.J.; Orimo, S.-I. Stable Interface Formation between TiS_2 and $LiBH_4$ in Bulk-Type All-Solid-State Lithium Batteries. *Chem. Mater.* **2015**, *27*, 5407–5416. [CrossRef]
58. Roedern, E.; Kühnel, R.-S.; Remhof, A.; Battaglia, C. Magnesium Ethylenediamine Borohydride as Solid-State Electrolyte for Magnesium Batteries. *Sci. Rep.* **2017**, *7*, 46189. [CrossRef]
59. Eriksson, T.; Andersson, A.M.; Bishop, A.G.; Gejke, C.; Gustafsson, T.; Thomas, J.O. Surface Analysis of $LiMn_2O_4$ Electrodes in Carbonate-Based Electrolytes. *J. Electrochem. Soc.* **2002**, *149*, A69. [CrossRef]
60. Pilli, A.; Jones, J.; Chugh, N.; Kelber, J.; Pasquale, F.; LaVoie, A. Atomic layer deposition of BN as a novel capping barrier for B_2O_3. *J. Vac. Sci. Technol. A* **2019**, *37*, 041505. [CrossRef]
61. Yu, X.; Xue, L.; Goodenough, J.B.; Manthiram, A. A High-Performance All-Solid-State Sodium Battery with a Poly(ethylene oxide)–$Na_3Zr_2Si_2PO_{12}$ Composite Electrolyte. *ACS Mater. Lett.* **2019**, *1*, 132–138. [CrossRef]
62. Xu, X.; Li, Y.; Cheng, J.; Hou, G.; Nie, X.; Ai, Q.; Dai, L.; Feng, J.; Ci, L. Composite solid electrolyte of Na_3PS_4-PEO for all-solid-state SnS_2/Na batteries with excellent interfacial compatibility between electrolyte and Na metal. *J. Energy Chem.* **2020**, *41*, 73–78. [CrossRef]
63. Zhang, Z.; Zhang, Q.; Ren, C.; Luo, F.; Ma, Q.; Hu, Y.-S.; Zhou, Z.; Li, H.; Huang, X.; Chen, L. A ceramic/polymer composite solid electrolyte for sodium batteries. *J. Mater. Chem. A* **2016**, *4*, 15823–15828. [CrossRef]